Planning, Calibration and Collision-Avoidance for Image-Guided Radiosurgery

Achim Schweikard [⋆†] Mohan Bodduluri [⋆] Rhea Tombropoulos [⋆ ‡] John R. Adler [†]
[⋆] Robotics Laboratory, Department of Computer Science
[†] Department of Neurosurgery
[‡] Section on Medical Informatics, School of Medicine
Stanford University, Stanford, CA. 94305,
[⋆] Accuray Inc., Santa Clara, CA. 95054
{as | rhea}@flamingo.stanford.edu

Abstract: *In radiosurgery a moving beam of radiation is used as an ablative surgical instrument to destroy brain tumors. Classical radiosurgical systems rely on rigid skeletal fixation of the anatomic region to be treated. This fixation procedure is very painful for the patient and limits radiosurgical procedures to brain lesions. Furthermore, due to the necessity of rigid fixation, radiosurgical treatment with classical systems cannot be fractionated. A new camera-guided system capable of tracking patient motion during treatment has been built to overcome these problems. The radiation source is moved by a six degree-of-freedom robotic arm. In addition to offering a more cost effective, less invasive, and less painful treatment, the robotic gantry allows for arbitrary spatial motion of the radiation source. Based on this feature we can treat non-spherical lesions with accuracies unachievable with classical radiosurgical systems. The system introduces a new class of radiosurgical procedures, called* non-stereotactic, *or* image-guided *radiosurgery. At the heart of these procedures are algorithms for planning both a treatment and the corresponding beam motion, given the geometric description of the tumor shape and relative locations in the particular case.*

1 Introduction

In radiosurgery, brain tumors (and other brain lesions) are destroyed by moving an intense beam of radiation [2, 6]. A necrotic dose is delivered to a tumor by cross-firing from multiple directions, to reduce the amount of energy deposited in healthy brain. The radiosurgical treatment consists of several phases. First, a precise 3D map of the anatomical structures in the area of interest (for instance, the brain) is constructed using computed tomography (CT) and magnetic resonance (MR). Next a motion path for the radiation beam is computed to deliver a dose distribution that the surgeon finds acceptable (taking into account a variety of medical constraints). Finally, a jointed mechanism moves the radiation source according to this path.

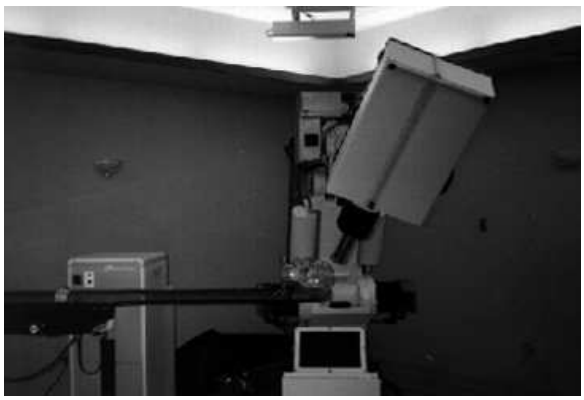

Figure 1: Robotic radiosurgical system, patient couch, on-line x-ray vision system

A new radiosurgical system has been built to overcome limitations of earlier systems. The new system is based on an on-line x-ray vision system and a 6 degree-of-freedom manipulator moving a compact and light weight linear accelerator.

2 System Overview

The system consists of the following components (Fig. 1):

• *Radiation source:* A novel compact and light-weight linear accelerator running at high frequency generates a 6 MV photon beam.

• *Mechanical gantry:* A GM-Fanuc 420 manipulator with six degrees-of-freedom moves the linear accelerator during treatment.

• *Treatment planning:* Geometric planning algorithms are at the heart of the new system. A beam path is computed given the constraints placed by the desired dose distribution. The beam path must observe additional constraints, i.e. the path must be collision-free and must not obstruct the surveillance and on-line vision subsystems.

• *Surveillance:* An ultrasonic system surveys the position of the robot and the linear accelerator during treatment.

• *Static and Dynamic Imaging:* CT and MR scanners acquire pre-operative images of the brain. An online vision system with two orthogonal x-ray cameras takes images of the patient's skull twice every second and computes the patient's position by correlating the images to precomputed radiographs. Small movements of the head are compensated for by a corresponding motion of the manipulator arm. Larger movements cause the radiation process to be interrupted.

During treatment, the linear accelerator is moved in point-to-point mode through a series of configurations. At each configuration, the beam is activated for a small time interval δt, while the arm is held still.

Currently, the beam has circular cross-section the radius of which remains constant throughout a given treatment. However, this radius is initially set between 5mm and 40mm by mounting a *collimator* (lead inset for beam focusation) to the radiation source.

The new system offers the following advantages over earlier radiosurgical and radiotherapeutical systems (see e.g. [7, 9, 10]):

- The tissue does not have to be fixed in space. In earlier radiosurgical systems this was done with stereotaxic frames. Besides being very painful for the patient, this fixation was only possible for the lesions in the head, so the use of radiosurgical methods was limited.
- Treatment can be fractionated, i.e. the total dose can be delivered in a series of 2-30 treatments, where only a small dose is delivered during each treatment. Fractionation has turned out to be highly effective in radiation therapy, but could not be used in radiosurgery due to the necessity of rigidly fixing the tissue in space.
- Based on geometric planning algorithms the radiation dose can be focused within the lesion with high accuracy so that healthy tissue can be protected, and side effects of radiation can be reduced dramatically. In particular, our algorithms allow for generating dose distributions with prescribed non-spherical isodosic surfaces and high homogeneity.

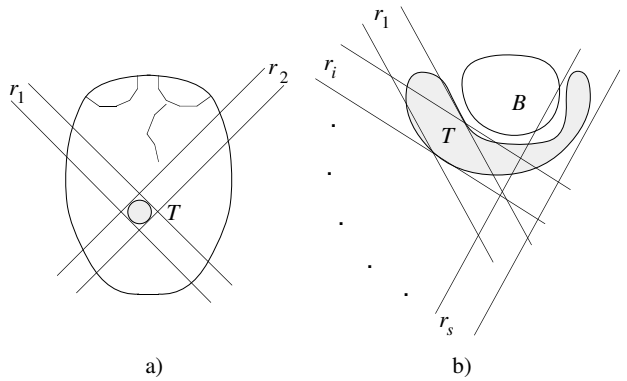

Figure 2: Cross-firing at a tumor

A prototype of the new system has been installed at Stanford Medical Center. The use of the system for clinical investigation was approved in February 1994.

3 Geometric Treatment Planning

The objective of treatment planning is to find a motion suitable for treating the particular condition presented by a patient. This planning problem is illustrated in Fig. 2. Fig. 2-a schematically depicts an axial cross-section of the brain with a circular tumor T. If T is irradiated from only one direction r_1, the healthy tissue along the beam absorbs approximately the same dose as the tumor. If, instead, we use two beam directions, r_1 and r_2, the dose deposited in the tumor is approximately twice the dose in healthy tissue. Using more beam directions can lead to further improvements of the dose distribution, and a very sharp drop-off of the dose in the tissue surrounding the (spherical) tumor region can be achieved. In this type of treatment, the axes of all beams cross a single point in space, called the *isocenter*. However, for tumors of non-spherical shape this single-isocenter treatment procedure is problematic (fig. 2-b).

Treatment planning has to take into account the following constraints.

- The region receiving high dose should match the tumor region. To protect healthy tissue, sharp

dose drop-off should be achieved in the healthy tissue surrounding the tumor.

- Certain anatomic structures, (i.e. optic nerves, arteries, brain stem) are very critical and/or radiation sensitive. The dose in such critical regions should be very small.
- Dose homogeneity; for certain lesions, it is essential that the dose inside the lesion be uniform. The dose in healthy non-critical tissue should also be uniform.

Planning a radiosurgical or radiotherapeutical treatment is difficult and time-consuming. In many cases, the constraints characterizing an adequate dose distribution cannot be met simultaneously. Our method for computing a suitable treatment plan proceeds in two steps:

- Beam selection: beams are selected according to the given tumor shape. The selection uses a reachability model of the manipulator workspace.
- Beam weighting: an intensity or *weight* is assigned to each beam. The weight is given by the duration of beam activation.

4 Selecting Beam Configurations

Spherical Tumors: First assume the tumor is spherical, with center p and radius r. We set the radius of all beams to r. The beam configurations are then selected in the following way. The axes of all beams cross the tumor center p. (p is the isocenter.) We consider beam directions determined by vertices of a regular (Platonic) polyhedron centered at p. The choice orientation of this polyhedron is problematic if there are critical healthy structures in the tumor vicinity. Furthermore there is no such regular polyhedron with more than 20 vertices. A more even distribution is obtained using more directions. The methods in [14] provide point grids on spheres which are adequate for our purposes. Our planning method thus uses a large set of beams (typically $n \geq 300$) for a single sphere, and addresses the presence of critical regions not during the beam selection phase, but during the beam weighting phase.

Ellipsoidal Shapes: While the scheme in the previous paragraph gives both very sharp dose drop-off around a sphere-shaped lesion and sufficient homogeneity, generalizations of this scheme for treating non-spherical tumors are not obvious.

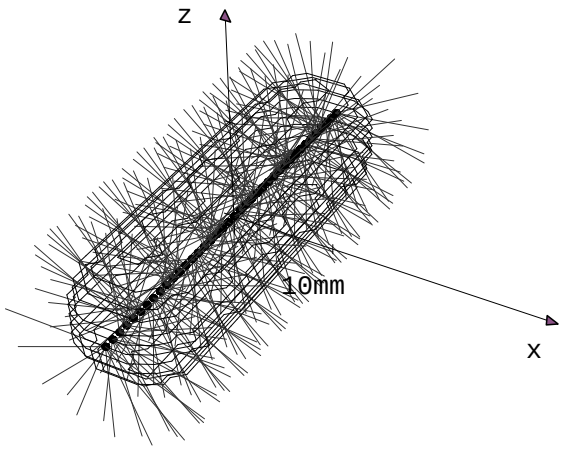

Figure 3: Isodosic surface, beam directions. Region inside surface absorbs 50% or more of maximum dose

A first attempt is to use two spheres instead of a single sphere, where each sphere is treated independently. However, it is generally difficult to cover an arbitrary tumor shape with spheres, such that the volume of overlap with the tumor environment is small, and the entire shape is covered. This is aggravated by the fact that the two spheres should not intersect, since this would yield very inhomogeneous dose distributions, i.e. high dose (so-called hot spots) in the intersection region of the spheres and/or insufficient coverage of the tumor region. Studies on complication rates show that hot spots, even inside the tumor, should be avoided if at all possible.

However, a simple generalization of the above single sphere method is obtained in the following way. Instead of using a single isocenter, we place a series of isocenters evenly spaced along a line segment. Each such isocenter is treated in the same way as a single isocenter. Central to this approach is the fact that each sphere receives very low dose, and many spheres are overlaid. In this way we can avoid hot spots in the intersection of two spheres.

The dose distribution resulting from such a motion as well as isocenter points and beam directions for generating this distribution are shown in figure 3. The figure shows a 50% isodosic surface, i.e. the region inside the surface receives 50% or more of the maximum dose.

There are several problems with this method:

1. If we use the same set of directions for all isocenters thus chosen, many of the beams will be parallel. Accumulated dose fall-off from such beams

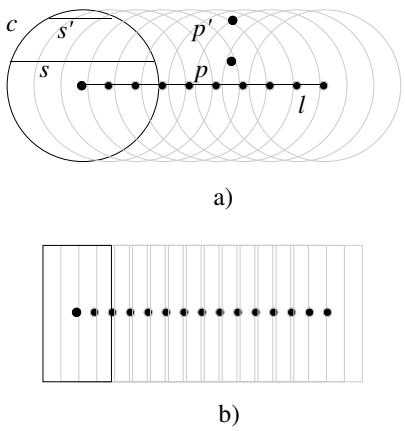

Figure 4: Sweep-motion a) beam has circular cross-section b) Beam cross-section is rectangular

will cause dose inhomogeneity in the surrounding tissue.

2. Dose inhomogeneity in the tumor may occur. The dose in the tumor center will be much higher than the dose along the tumor boundary, as illustrated in example 1 below. This inhomogeneity is in large part due to the cylindrical beam shape.

To address the first problem, we choose rotated beam sets for each isocenter. In practice rotating the entire beam set aimed at one isocenter by a fixed amount is equivalent to choosing each individual beam direction from a finer spherical point grid. Furthermore, instead of using several beams for each isocenter, we can use a larger set of isocenters, evenly spaced on a line segment and a single beam (from the finer sphere grid) for each such isocenter. Thus we place a single beam through each isocenter point along the line segment. Each beam direction is then chosen (in random order) from a fine grid of points on the unit sphere.

The second problem can be addressed in several ways. The following example shows that the mentioned problem is related to the collimator shape.

Example: Fig. 4-a shows the cross-section of a cylindrical beam swept along a line segment l. The beam axis is orthogonal to the plane of cross-section. The beam cross-section is a circle c. The point p will absorb higher dose than point p' during this sweep-motion. The dose at these points will be proportional to the length of the segments s and s', thus causing substantial inhomogeneity.

A beam with rectangular cross-section avoids this problem. (figure 4 b).

General Shapes: The above approach is restricted to the pseudo-cylindrical shapes shown in figure 3 and shapes obtained from bending such shapes. A direct generalization of this scheme is the following. With an algorithm in [14], we compute a grid of n points on the *tumor surface*. Each such point is now treated as an isocenter. As above, a single beam is placed through each isocenter. This scheme addresses both the first and the second of the mentioned problems: Accumulation along certain principal directions is avoided by using a fine grid. Accumulation of high dose in the tumor center is avoided by placing isocenters on the tumor surface. To achieve homogeneity, the point grid on the input surface can be expanded or retracted interactively. A path thus generated is refined by computing beam weights.

5 Computing Beam Weights

During the second planning step, weights are assigned to each of the previously selected beams. Let $C_1, \ldots, C_n$ denote the cylindrical beams at the n selected configurations.

Our method will assign a dose value $w_i \geq 0$ to every C_i. w_i is a factor specifying activation duration at the particular (static) beam configuration. The values $w_1, \ldots, w_n$ determine a distribution D, defined as follows. If p is a point and $C_{i_1}, \ldots, C_{i_k}$ are the cylinders containing p, then $D(p) = w_{i_1} + \cdots + w_{i_k}$. (This definition provides a coarse model for photon beam characteristics. Refinements described in [12] allow for a more accurate representation of these characteristics.)

We consider two disjoint regions T (for tumor) and H (for healthy tissue), with the following constraints: the dose delivered at each point in T must be larger than some value α, while the dose at each point of H must be below β ($\beta < \alpha$). The n cylinders, T, and H define an arrangement of *cells* in space. Each cell is defined as a maximal connected set not containing any piece of the boundaries of regions T and H or the cylinders. For each cell we compute a *label*. A cell κ in cylinders $C_{i_1}, \ldots, C_{i_k}$ has label $l = \{i_1, \ldots, i_k\}$.

The calculation of $w_1, \ldots, w_n$ reduces to finding a point in the intersection of two n-dimensional polyhedral sets: If κ is in T and labeled by $\{i_1, \ldots, i_k\}$ then κ determines the inequality:

$$\alpha \leq w_{i_1} + \cdots + w_{i_k}.$$

A cell κ' labeled by $\{j_1, \ldots, j_{k'}\}$ in H gives:

$$\beta \geq w_{j_1} + \cdots + w_{j_{k'}}.$$

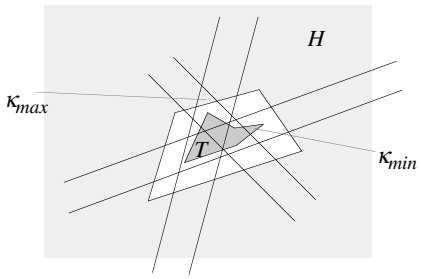

Figure 5: Regions T, H, minimal and maximal cell κ_{min} resp. κ_{max}.

The inequalities for all cells in T determine a convex polyhedral set P_α. Similarly, the inequalities derived from the cells in H determine a polyhedron P_β. If P_α and P_β intersect, any point $(w_1, \ldots, w_n)$ in the intersection gives a dose distribution that satisfies the given constraints. Otherwise, the problem admits no solution.

More generally, we can specify several healthy critical or non-critical regions $H_1, \ldots, H_q$ marked by distinct maximal doses $\beta_1, \ldots, \beta_q$. We then obtain polyhedra $P_\alpha, P_{\beta_i}, \ldots, P_{\beta_q}$. Any point $(w_1, \ldots, w_n)$ in the intersection of these polyhedra determines a dose distribution that satisfies the input constraints.

The intersection of the polyhedral sets $P_\alpha, P_{\beta_1}, \ldots, P_{\beta_q}$ is another n-dimensional convex polyhedral set. Extreme points of this set can be computed, allowing us to deal directly with optmization criteria (e.g., in addition to satisfying the input constraints defined by $\alpha, \beta_1, \ldots, \beta_q$, minimize the dose delivered to some region H_i).

Reducing the number of inequalities: We consider two inequalities deriving from two cells κ and κ' in T. Let $L = \{i_1, \ldots, i_k\}$ and $L' = \{j_1, \ldots, j_{k'}\}$ be the labels of κ and κ'. If $L \subset L'$, then the inequality given by κ implies the inequality given by κ', since all w_i are positive or null. A T-cell is called *minimal*, if its label is not a superset of any other T-label (figure 5). Similarly, a cell in H_i is called *maximal*, if its label is not a subset of any other label in H_i. Thus, in the above polyhedral intersection test, we need only to consider minimal T-cells and maximal H-cells.

6 Kinematics and Collision Avoidance

The beam configurations selected by the planning system must be organized into a sequence defining a collision-free path of the linear accelerator. For safety reasons, we currently do not use optimization methods

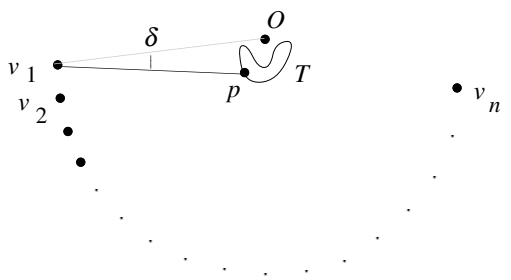

Figure 6: Origin O, target region T, tool-center points $v_1, \ldots, v_n$ for hard-coded nodes

for computing this sequence. Instead, we use a hard-coded sequence of beam configurations, called *nodes*. A fixed motion connecting the nodes provides a path template. An essential feature of the beam selection method is the following: Beam configurations can be selected in such a way that the deviation between the hard-coded path template and the treatment beams calculated for an individual patient is small and upper-bounded. For all node configurations the beam axis crosses the work space origin. A node is thus simply given by a tool center point placement. We use tool center points on a sphere of appropriate radius centered at the origin. For each node we compute a local joint space. Thus, angle limits within which the arm and the accelerator can be moved without colliding or getting into the line of sight of a camera are associated with each node. To compute treatment beams given the particular tumor shape and location as described in section 3, we connect isocenter points to the tool center points of nodes. Thus each treatment beam is given by an isocenter point and the tool center point for a node. Given reasonable bounds for the tumor size we can assume that isocenter points are close to the workspace origin. Since the source-target distance for the beam is large, we can ensure that the angular deviation between a hard-coded node and associated treatment beam configurations remains below a fixed threshold, and within the local joint space of the node (figure 6).

The placement of a cylinder beam in space is kinematically redundant. The beam can be translated along and rotated about its axis without changing spatial placement. Thus a cylinder has four degrees of freedom. The range of beam directions should be as large as possible to allow for homogeneous distributions. A simulating program is used to determine tool center points for nodes covering a large portion of a half-sphere (fig-

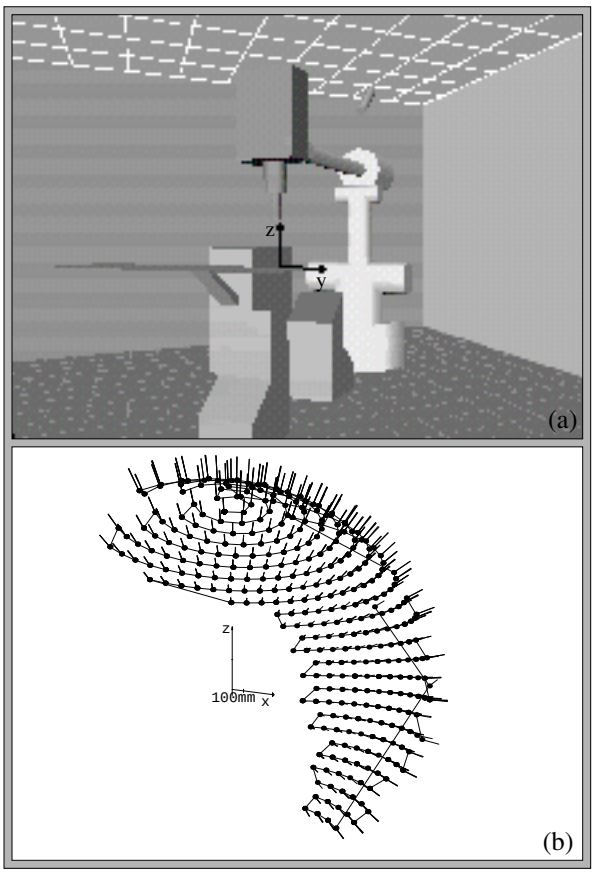

Figure 7: Path template connecting node configurations

ure 7). The beam widens with source-target distance. By placing tool center points for all nodes and treatment points on a sphere we can ensure that all beams have nearly constant and equal radius in tissue.

Effector orientation is represented by three Euler angles such that the last of these angles gives the rotation about the beam axis. For each node an appropriate value for this angle is computed in such a way that arm posture changes along the path can be avoided.

For verification the path in Fig. 7-b was executed and a photographic film in a water phantom (plexiglass reconstruction of a skull, placed at the end of the patient couch in figure 1) was exposed to the generated radiation.

During execution of the path in Fig. 7-b) an equal dose value was delivered at each node, with the beam axis aimed at the work space origin. The restrictions in the workspace result in a penumbra along the horizontal direction in Fig. 8 c) and d). A total of 6000 cGy was delivered at 300 nodes, resulting in a total execution

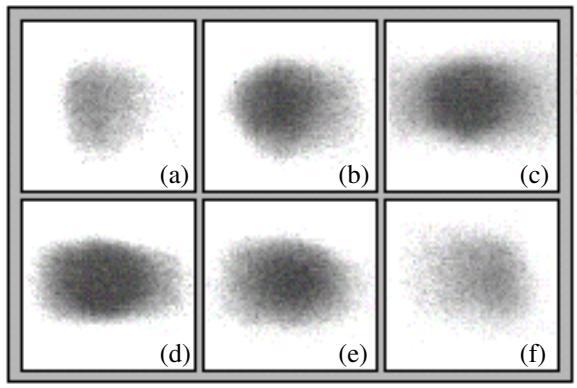

Figure 8: Photographic film phantom for spherical distribution (axial cross-sections)

time of 1 hour.

7 Calibration

The positioning accuracy of the mechanical gantry is much lower than the repeating accuracy. The radiation source must remain at sufficient distance from the tissue to be irradiated. Small inaccuracies in positioning the radiation source are thus amplified and may cause inaccuracies in target localization. Thus the hard-coded motion path was calibrated in the following way. An optical crystal was placed at the work space origin. A laser beam pointing along the beam central axis was placed in the radiation source. The crystal is activated when touched by the laser beam. Activation intensity can be read from the crystal, thus giving a measurement for placement accuracy. The calibration process considers each node separately. The end effector is placed at grid points in a small local joint space surrounding the node. At each grid point the laser is activated and a measurement is taken from the crystal. For the given node we can thus find joint angle offsets placing the beam in such a way that the beam axis crosses the origin. The angular deviation between treatment points and hard-coded nodes is small, and we use the offsets thus computed as offsets for the treatment beams as well. A bound of 0.3 mm for inaccuracies was determined experimentally for isocenter points close to the origin.

8 Planning System

A treatment planning system with 3D graphical user interface based on the above beam selection and weighting methods is incorporated into the new system. It

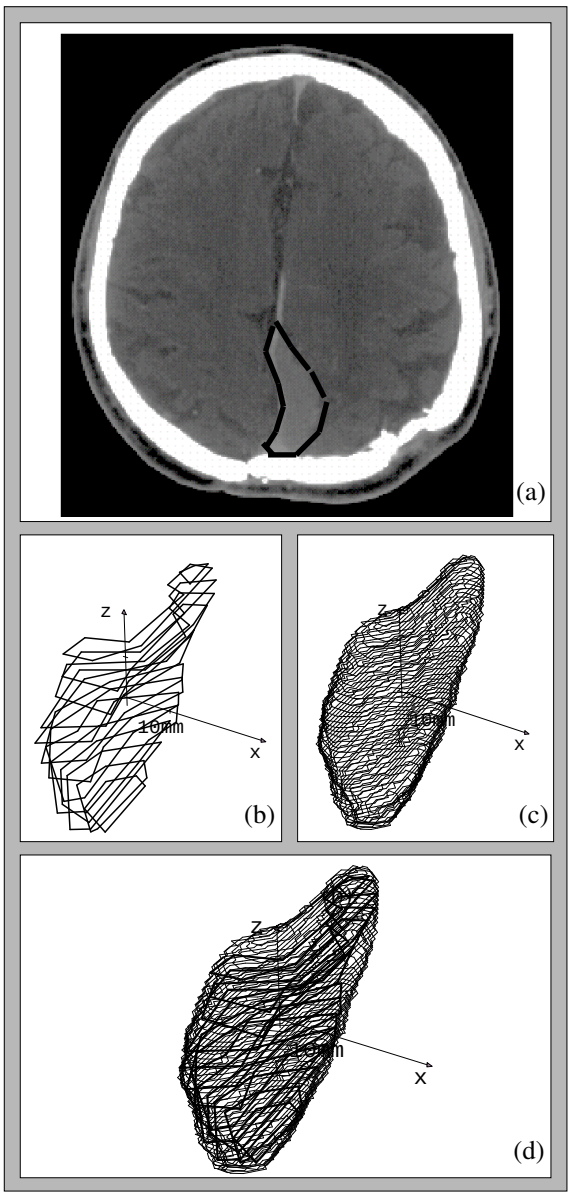

Figure 9: Sample case (Stanford Medical Center). (a) Axial CT with tumor delineated in black (b) 3D representation of tumor delineation (c) Isodosic surface (d) Isodosic surface overlaid on tumor reconstruction

is designed to enable the surgeon to make use of the system flexibility.

Inputs: The tumor and critical tissues are described as polyhedra. The regions of interest are delineated by polygons in the MR images showing axial, sagital, or coronal cross-sections of the brain. These polygons are thickened between two cross-sections, and a 3D reconstruction of the tumor shape is computed. The ra-

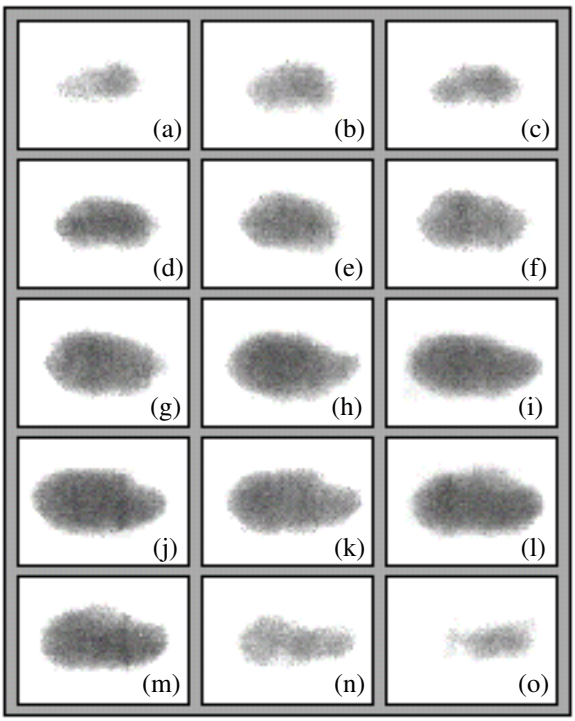

Figure 10: Film phantom for sample case in Fig. 9, showing the shape of the region receivinghigh dose. Film slices in the phantom are arranged in the same spatial structure as the tomographic images.

dius r of the (cylindrical) beam and the number (n) of beam configurations are given as input. The beam selection method in section 3 in combination with the above collision avoidance method is invoked to compute a set of beam directions corresponding to the input tumor shape and location. To compute beam weights, our implementation uses a modified simplex algorithm to find a point within the intersection region of k $n-$dimensional polyhedra.

A test series for the new system was carried out to evaluate the possibilities of generating prespecified dose distributions. In the test series, cases treated during a comparison period with an earlier system for frame-based stereotactic radiosurgery [7] were considered. In each case data for the actual treatment performed were retrieved. Plans for the same cases were then computed with our new planning system. The comparison is based on photographic film phantom studies in water, dose-volume histograms, as well as 2D and 3D dose visualization paradigms. The results of the test series and variants of the above methods are discussed in [12].

An example is shown in figures 9 a-d and 10. Fig. 9-a

shows an axial cross-section of the brain for a 69 year old patient presenting a large non-spherical tumor of the falx cerebri, delineated in the cross-section. Fig. 9b shows the 3D reconstruction of the tumor outline. A regular grid of 600 points was expanded on a surface reconstruction, giving isocenter points. Fig. 9c) shows the 50% isodosic surface resulting from the computed motion. Fig. 9d) overlays the input tumor shape with the generated isodosic surface to illustrate the matching between input and output shapes. For verification, the motion was executed exposing a photographic film phantom (figure 10). The phantom shows a close matching between the input tumor shape and the actual shape of the region receiving high radiation dose.

9 Conclusion

A prototype of the new system has been installed at Stanford Medical Center and the use of the system for clinical investigation has been approved. Systems will soon be installed at several major medical research institutions.

The methods described divide treatment planning into two steps: (1) Selection of beam configurations. (2) Computation of dose weights for these configurations. For the latter step, we proposed a general theoretical approach. The evaluation of the planning methods gives very encouraging results. Improved methods could include other collimator geometries and corresponding generalizations of the planning paradigms. The planning method relies on weighted arrangements in 3D space. This is not limited to cylinders, and seems appropriate for treatment planning in conventional radiation therapy as well.

It is likely that the new systems will allow for radiosurgical treatment of tumors outside the brain, including tumors for which no treatment is currently available. In particular, extensions are desirable for very radiation-resistant tumors and cases in which conventional radiation therapy would cause too much damage to healthy tissue and is not applicable.

Acknowledgments: This research is funded in part by the Sheik Enany Fund, Lorraine Ulshafer Fund and by the National Library of Medicine (LM-05305 and LM-07033). The authors thank Joe Depp, Martin Murphy and Bo Preising of Accuray Corp. for comments and suggestions.

References

[1] Barth, N. H. An Inverse Problem in Radiation Therapy. *Intern. J. Radiation Oncology Biol. Phys.*, 18:425–431, 1990.

[2] Betty, O. O., Munari, C., and Rosler, R. Stereotactic Radiosurgery with the Linear Accelerator: Treatment of Arteriovenous Malformations. *Neurosurgery*, 24(3):311–321, 1989.

[3] Brahme, A. Optimization of stationary and moving beam radiation therapy techniques. *Radiother. Oncol.*, 12:127-140, 1988.

[4] Cormack, A. A problem in rotation therapy with x-rays. *Int. J. Radiat. Oncol. Biol. Phys.*, 13:623-630, 1987.

[5] Halperin, D. and Yap, C.K. Combinatorial Complexity of Translating a Box in Polyhedral 3-Space *9th Annual ACM Symp. on Computational Geometry*, 29–37, 1993.

[6] Larsson, B. et al. The High Energy Proton Beam as a Neurosurgical Tool. *Nature*, 182:1222–1223, 1958.

[7] Lutz, W., Winston, K. R., and Maleki, N. A System for stereotactic radiosurgery with a linear accelerator. *Int. J. Radiation Oncology Biol. Phys.*, 14:373–381, 1988.

[8] Murtagh, B. A., Saunders, M. A., Minos 5.4 user's guide. Technical Report SOL 83-20R, Dept. of Operations Research, Stanford University, 1983.

[9] Podgorsak, E. B., et al. Dynamic Stereotactic Radiosurgery *Intern. J. Radiation Oncology Biol. Phys.*, 14:115–126, 1988.

[10] Rice, R. K., et al. Measurements of Dose Distributions in Small Beams of 6 MeV X-Rays. *Phys. Med. Biol.*, 32:1087–1099, 1987.

[11] Schweikard, A., Adler, J. R., and Latombe, J. C., Motion Planning in Stereotaxic Radiosurgery. *Proc. IEEE Int. Conf. Robotics and Automation*, Atlanta, GA, May 1993, 1909–1916. (Extended version to appear in *IEEE Tr. Robotics and Automation.*)

[12] Schweikard, A., Tombropoulos, R. Z., Kavraki, L., Adler, J.R., and Latombe, J.C., Treatment Planning for a Radiosurgical System with General Kinematics. *Proc. IEEE Int. Conf. Robotics and Automation*, San Diego, CA, May 1994, 1720–1727.

[13] Troccaz, J. et al. Conformal External Radiotherapy of Prostatic Carcinoma: Requirements and Preliminary Results, Rep. No. 912I, TIMC-IMAG, Faculté de Médecine, Grenoble, 1993.

[14] Turk, G. Re-Tiling Polygonal Surfaces. *Computer Graphics*, 26(3):55–64, 1992.